

Coherent Polarization Transfer through Sub-wavelength Hole Arrays

Martin P. van Exter, Erwin Altewischer, and J.P. (Han) Woerdman

Huygens Laboratory, Leiden University, 2300 RA Leiden, The Netherlands

mvexter@molphys.leidenuniv.nl

<http://www.molphys.leidenuniv.nl/~mvexter>

Abstract. We review a series of experiments on the optical properties of metal films perforated with arrays of sub-wavelength holes. A key experiment is the transfer of polarization entanglement under plane-wave/focused illumination, where we observed a conservation/degradation of the quantum entanglement. Surface plasmons play a prominent role in the observed extra-ordinary large transmission. This is demonstrated with two supporting experiments performed with classical light, investigating: (i) the polarization and angular dependent transmission through the arrays, (ii) the generation of coherent beams of surface plasmons. Both experiments prove the directionality and TM-character expected for surface plasmon modes on a hole array.

Keywords: surface plasmon, hole array, entanglement, polarization.

1 Hole Arrays in Metal Films

Arrays of sub-wavelength holes in metal films have attracted attention since the landmark experiment of Ebbesen et al. [1]. This experiment demonstrated an extra-ordinary large transmission, i.e., a transmission much larger than expected from the incoherent sum of the transmission per hole. The enhanced transmission was attributed to the resonant excitation of surface plasmon polaritons, briefly denoted as surface plasmons (SP), and the consecutive back-conversion into photons. This claim was first disputed by Henry et al. [2], who argued that the idea of plasmon-mediated transmission was not consistent with all observations, but is now commonly accepted. Most experiments performed over the past ten years, including the ones presented in this paper, support the prominent role of surface plasmons in the observed large transmission; see review paper of Garcia-de Abajo [3] and reference therein.

We have used square and hexagonal arrays of holes with an identical layer structure, comprising a 200 nm-thick gold film evaporated onto a glass substrate, with a 2-nm thin Chromium or Titanium layer in between to improve the attachment. The square array was produced with e-beam lithography on a quartz substrate; it has a lattice constant $a = 700$ nm and an average hole diameter of 200 nm. The hexagonal array was created with a focused ion beam on a

BK7 substrate; it has a lattice constant $a = 886$ nm and an average hole diameter of 180 nm. The two main graphs of Fig. 1 show the transmission spectra at normal incidence. That these spectra are practically independent of the optical polarization proves the high quality/uniformity of the arrays; even a 1% difference between the lattice spacings in the principle directions would have been noticed. At non-zero angle of incidence these transmission spectra change and acquire the polarization dependence that is characteristic of plasmon-assisted transmission [4]. The observed asymmetric spectral line shapes results from interference between a resonant and non-resonant contribution, together denoted as a Fano resonance [5]. The former is attributed to the resonant excitation of surface plasmons; the later is attributed to the (generally much weaker) direct transmission through the holes.

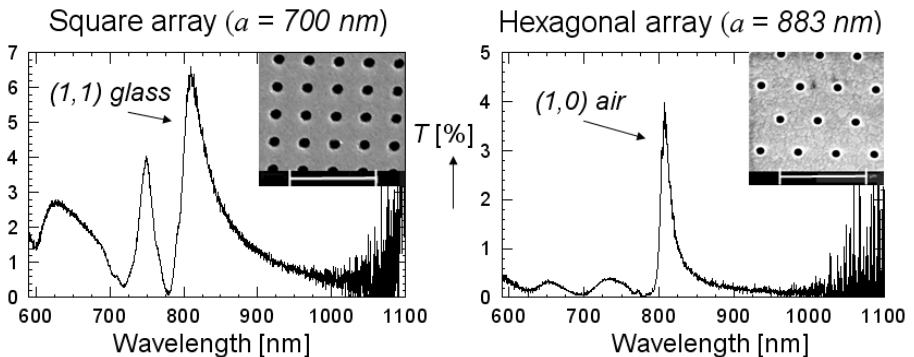


Fig. 1. Transmission spectra of a square and hexagonal array for illumination at normal incidence. The insets show SEM images; the indicated ruler is 2 μm .

The spectral resonances in Fig. 1 result from coupling to surface plasmon modes with different wave vectors, propagating either on the top or bottom interface of the metal film. These modes can be labeled by their mode number (N, M), being the integer multiple of the lattice wave vectors that the SPs acquire upon excitation, and their location. For a square array illuminated at normal incidence this labeling yields the relations

$$\frac{2\pi}{a} \sqrt{N^2 + M^2} = k_{\text{sp}} = \sqrt{\frac{\epsilon_1 + \epsilon_2}{\epsilon_1 \epsilon_2}} \frac{\omega}{c}, \quad (1)$$

where ϵ_1 and ϵ_2 are the relative dielectric constants of the dielectric and the metal, respectively. The equation on the righthand side applies to any SP resonance; the optical confinement at the interface is guaranteed by the relation $\Re(k_{\text{SP}}) > \sqrt{\epsilon_1} \omega/c$, where \Re denotes the real part; the optical losses can be incorporated either in the imaginary part of k_{SP} or ω . The equation on the lefthand side applies only to square arrays; for hexagonal arrays it changes into $[4\pi/(\sqrt{3}a)]\sqrt{N^2 + N.M + M^2}$. Based on these equations, one can easily associate the dominant $\lambda \approx 810$ nm transmission peak of the square hole to the

(1, 1) SP mode on the quartz-metal interface; the weak $\lambda \approx 747$ nm corresponds to the (1, 0) SP mode on the air-metal interface. The $\lambda \approx 807$ nm transmission peak of the hexagonal array results from the (1, 0) SP mode on the air-metal interface. The sharper spectral structure of this mode as compared to the dominant resonance in the square array indicates that its losses are smaller, presumably due to its air-based character, its hexagonal geometry, and its somewhat smaller holes.

2 Plasmon-Assisted Transmission of Entanglement

When the large transmission through sub-wavelength hole arrays is interpreted as a conversion from photons to surface plasmons and back, one might wonder whether fragile properties such as quantum entanglement between photons survive this conversion. The entanglement could for instance be degraded if the transmission acts as a measurement that leaves ‘which-way’ information in the system. We have addressed this issue in ref. [4], where we show that polarization entanglement is only conserved if the array is illuminated with a weakly-focused beam; it is lost under strong focusing, due to a transfer of polarization information to the spatial degrees of freedom.

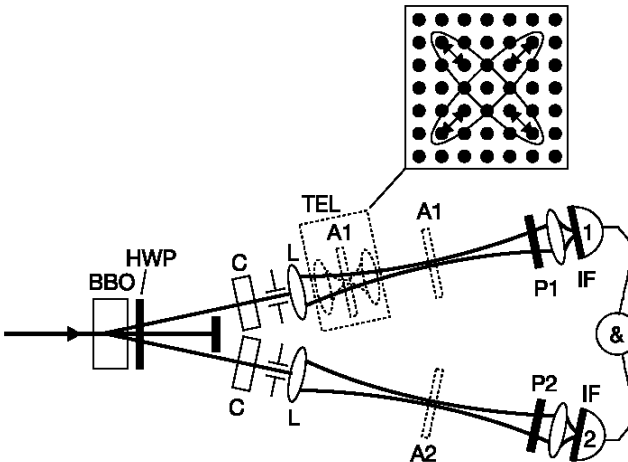


Fig. 2. Experimental setup used to generate polarization-entangled photon pairs (top and bottom beams) from an incident pump laser focused in a BBO crystal. Polarization compensation and spatial and spectral filtering is performed with a half-wave plate (HWP), compensating crystals (C), apertures, and interference filters (IF). We measure the rate of coincidence detection in photon counters 1 and 2 with a fast AND gate (indicated by the & symbol) for various settings of the polarizers P1 and P2. The inset shows the expected intensity profile behind array A1 under focused illumination; the arrows indicate the polarization directions; the central region is unpolarized.

Figure 2 shows the experimental setup. Entangled photon pairs are generated in a nonlinear optical crystal (BBO), where spontaneous parametric down-conversion leads to a sporadic break-up of a blue ($\lambda = 406.7$ nm) pump photon into a pair of red ($\lambda \approx 813$ nm) photons. After spatial and spectral filtering and polarization compensation, the selected photon pairs are polarization entangled [6]. This means that the polarization state of neither of the individual photons is fixed, but a (projective) polarization measurement on photon 1 will also fix the polarization of photon 2. The amount of polarization entanglement can be quantified by measuring the pair coincidence detection rate for various settings of the polarizers (P_1 and P_2). More specifically, the relative amount of (VV/HH) over (VH/HV) pairs yields the biphoton fringe visibility V_{0° . Likewise, the relative amount of (DD/AA) over (AD/DA) pairs, where D/A refers to the $45^\circ/-45^\circ$ orientation, yields the visibility V_{45° . The observation $V_{0^\circ} \approx V_{45^\circ} \approx 100\%$ is a proof of quantum entanglement, as this relation cannot be obeyed for sources that exhibit only classical polarization correlations [7].

Table 1 shows the measured visibilities V_{0° and V_{45° observed under various illumination conditions (plane-wave or focused) with zero, one or two square hole arrays in the beams. The three top rows demonstrate the true quantum nature of our source, via the relation $V_{0^\circ} \approx V_{45^\circ} \approx 100\%$, and the conservation of polarization entanglement under plane-wave transmission through the hole array(s). The four bottom rows demonstrate how the entanglement is degraded when the hole arrays are illuminated with a focused beam (numerical aperture ≈ 0.13). In hindsight, this second observation, of entanglement degradation under focused illumination, is the most surprising and the main reason why ref. [4] made it into Nature. It shows among others that the optical transmission through a hole array is quite different from the transmission through a simple absorbing media or the reflection from a (lossy) mirror. The former leads to a transfer of polarization to spatial information (see below), whereas the later does not. The observed visibilities indicate a preference (= less entanglement degradation) for polarizations aligned with the diagonal of the square array, in agreement with the $(1, 1)$ (diagonal) character of the excited SP mode. Note how this preference appears naturally under all four experimental conditions.

Table 1. Conservation and degradation of polarization entanglement under different experimental conditions. The amount of polarization entanglement is quantified via the biphoton fringe visibilities V_{0° and V_{45° (see text).

Experiment	V_{0°	V_{45°
Without arrays	99	97
Array 1 only, approx. plane-wave beam	99	97
Both arrays, approx. plane-wave beams	97	97
Array 1 only at 0° orientation, focused beam	73	87
Array 1 only at 45° orientation, focused beam	90	74
Two arrays at $(45^\circ, 45^\circ)$ orientation, focused beams	82	58
Two arrays at $(0^\circ, 45^\circ)$ orientation, focused beams	65	67

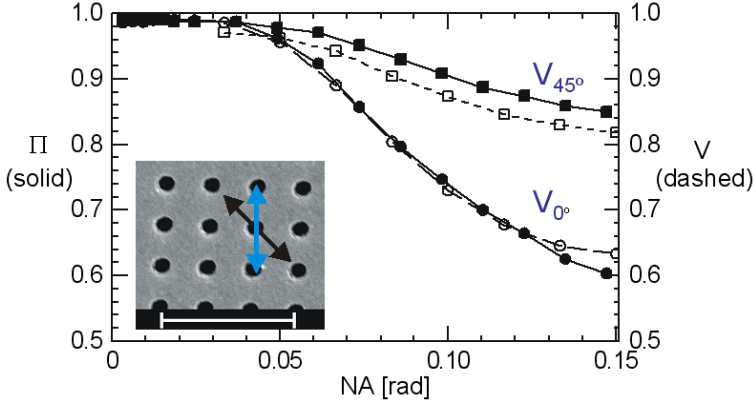


Fig. 3. Measured degree of polarization Π (solid lines and symbols) and biphoton visibilities V (dashed lines and open symbols) for transmission through a square array of holes as a function of the numerical aperture (NA) of the focused input for two different polarizations (0° and 45°) indicated by arrows in the SEM picture

Two essential ingredients are necessary for the transfer of quantum entanglement. First of all, the transfer should be coherent, preserving both amplitude and phase information. This requirement applies to the transmission through any static linear medium. Secondly, the transmission shouldn't provide ‘which-way’ information on the quantum-entangled degrees of freedom. The later requirement is violated for focused transmission of polarization entanglement through a hole array. The inset in Fig. 2 schematically shows how the polarization entanglement in a tightly-focused input beam affects the spatial profile of the output beam, which will be extended along the diagonals due to the propagation of the excited surface plasmons. This tentative explanation is confirmed by the experiments discussed in section 3 and 4. It is also supported by the observation that a similar polarization degradation occurs for transmission of a tightly-focused classical beam with a fixed polarization; the depolarization is now determined by measuring the (spatially-averaged) power behind a polarizer oriented either parallel or perpendicular to the incident polarization [9]. A comparison between the observed classical depolarization (for fixed input polarization) and the quantum decoherence (for quantum-entangled input) is presented in Fig. 3. A similar agreement was found for the hexagonal array [9].

3 Angle-Dependent Transmission

The optical transmission through hole arrays is fully specified by a single transmission amplitude matrix $t(\omega, \theta)$, which links the plane-wave components of the input and output field as

$$\begin{pmatrix} E_{x,out}(\omega, \theta) \\ E_{y,out}(\omega, \theta) \end{pmatrix} = \begin{pmatrix} t_{xx}(\omega, \theta) & t_{xy}(\omega, \theta) \\ t_{yx}(\omega, \theta) & t_{yy}(\omega, \theta) \end{pmatrix} \begin{pmatrix} E_{x,in}(\omega, \theta) \\ E_{y,in}(\omega, \theta) \end{pmatrix}. \quad (2)$$

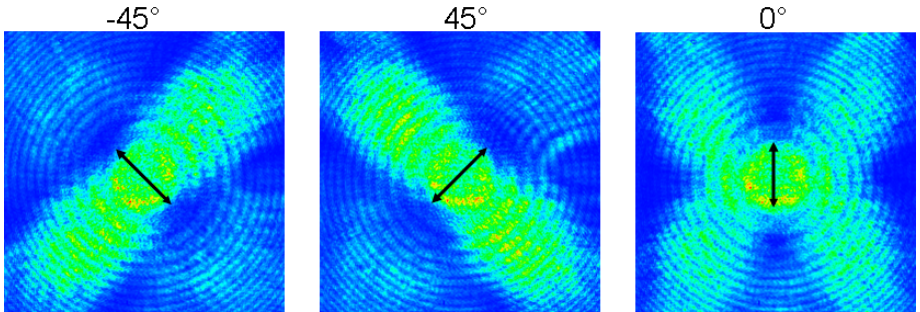


Fig. 4. Far-field transmission (in false-color intensities) of the square array under illumination at $\lambda = 810$ nm for three input polarizations (indicated by arrows and numbers). Each figure spans an angular range from -0.15 to $+0.15$ radians in both directions.

This relation is so simple because we consider only the zero-order diffraction at $\theta_{\text{out}} = \theta_{\text{in}}$ (θ symbolizes the incident angles in both directions). The crucial transfer matrix $t(\omega, \theta)$ contains the full polarization, frequency, and angle-dependence of the transmission; it thereby supplements the SP dispersion relation with information on polarization and losses.

Figure 4 shows the measured intensity transmission of the square array at $\lambda = 810$ nm as a function of the incident angle for three different input polarizations [8]. The $\pm 45^\circ$ figures show how the transmission persists to large angles of incidence only in a direction perpendicular to the polarization. By Fourier relation, the excitation is thus found to propagate mainly in the direction parallel to the polarization, as expected for SPs. The four diagonal structures observed under illumination with vertically-polarized light show that the transmission is indeed dominated by SPs propagating in the diagonal directions (in this case the (1,1) mode at the glass-metal interface). We attribute the absence of reflection symmetry along the diagonals to the admixture of a small transmission amplitude from the (1,0) air-metal mode at $\lambda \approx 747$ nm [8].

4 Beams of Surface Plasmons

The resonant excitation of SP beams, through constructive interference of SP waves generated at consecutive rows of holes in the array, can be easily observed by combining focused excitation with microscopic imaging of the transmitted light. For excitation of the square hole at $\lambda = 810$ nm we observed SP beams with intensity tails that decay exponentially over a length $\ell = 1.9 \pm 0.1 \mu\text{m}$ outside the Gaussian excitation spot. We also observed an intriguing Fano-type interference with the direct transmission in the central region [10]. No beams are generated in directions perpendicular to the incident polarization, an observation that again confirms the role of surface plasmons. The low-loss mode of the hexagonal array showed a more prominent propagation[11]. For excitation around its $\lambda \approx 807$ nm

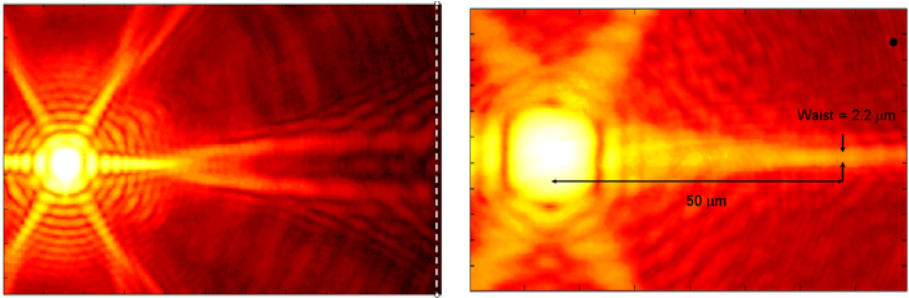


Fig. 5. Generation of surface plasmon (SP) beams by focused excitation in a hexagonal array of holes. Each figure covers a $85 \mu\text{m} \times 57 \mu\text{m}$ area. Intensities are displayed on a logarithmic (false color) scale that spans almost four orders of magnitude [11].

resonance we measure a decay length of $\ell = 8 \mu\text{m}$, whereas we find $\ell = 6 \mu\text{m}$ at $\lambda \approx 750 \text{ nm}$ and $\ell = 11 \mu\text{m}$ at $\lambda \approx 830 \text{ nm}$.

Figure 5 show two intriguing images of the transmitted intensity profile behind the hexagonal array. Both images were obtained with horizontal (x) polarization, making the beam in the x direction approximately $4\times$ as intense as the four beams emitted under other multiples of 60° . Both images were taken under slightly de-focused conditions, with the focus of the excitation laser at some $20/50 \mu\text{m}$ behind the hole array for the left/right figure. The transfer of coherence from the incident optical field to the in-plane propagating SP wave makes the generated SP beam convergent and produces displaced foci of approximately the same size as that of the incident beam. The focus in the righthand figure is displaced by as much as $50 \mu\text{m}$ from the (necessarily large) excitation spot, but still has a waist of only $2.2 \mu\text{m}$ as compared to the $1.6 \mu\text{m}$ waist of the incident beam. The excitation wavelength $\lambda = 830 \text{ nm}$ was red-shifted with respect to the resonance to limit the losses and increase the SP propagation length. The excitation wavelength in the left figure is at the resonance wavelength $\lambda = 807 \text{ nm}$. We attribute the observed breakup of the SP beam after $\approx 20 \mu\text{m}$ propagation to Bragg scattering from consecutive rows of holes; its precise structure changes considerably with wavelength [11]. The interference visible on the righthand side of this figure must be caused by the array's edge (dashed line), i.e., the transition from the array to a smooth metal film, but the details are not yet understood. The ring-like structure around the excitation spot, observed in both images, is due to a rather boring interference with light reflected inside the supporting glass substrate.

5 Summary and Conclusions

We have studied the polarization, angle, and wavelength dependence of square and hexagonal arrays of sub-wavelength holes in metal films. The prominent role of surface plasmons in the transmission is apparent in: (i) the entanglement

degradation under focused excitation, (ii) the combined polarization- and angle-dependence of the transmission, and (iii) the generation of beams of surface plasmons.

References

1. Ebbesen, T.W., Lezec, H.J., Ghaemi, H.F., Thio, T., Wolff, P.A.: Extraordinary Optical Transmission through Sub-wavelength Hole Arrays. *Nature* 391, 667–669 (1998)
2. Lezec, H.J., Thio, T.: Diffracted Evanescent Wave Model for Enhanced and Suppressed Optical Transmission through Subwavelength Hole Arrays. *Opt. Exp.* 12, 3629–3651 (2004)
3. Garcia de Abajo, F.J.: Light Scattering by Particle and Hole Arrays. *Rev. Mod. Phys.* 79, 1267–1290 (2007)
4. Altewischer, E., van Exter, M.P., Woerdman, J.P.: Plasmon-Assisted Transmission of Entangled Photons. *Nature* 418, 304–306 (2002)
5. Genet, C., van Exter, M.P., Woerdman, J.P.: Fano-type Interpretation of Red Shifts and Red Tails in Hole Array Transmission Spectra. *Opt. Commun.* 225, 331–336 (2003)
6. Kwiat, P.G., Mattle, K., Weinfurter, H., Zeilinger, A., Sergienko, A.V., Shih, Y.H.: New high-intensity source of polarization-entangled photon pairs. *Phys. Rev. Lett.* 75, 4337–4341 (1995)
7. Clauser, J.F., Horne, M.A., Shimony, A., Holt, R.A.: Proposed experiment to test local hidden-variable theories. *Phys. Rev. Lett.* 23, 880–884 (1969)
8. Altewischer, E., van Exter, M.P., Woerdman, J.P.: Polarization Analysis of Propagating Surface Plasmons in a Subwavelength Hole Array. *J. Opt. Soc. Am. B* 20, 1927–1931 (2003)
9. Altewischer, E., van Exter, M.P., Woerdman, J.P.: Quantum Decoherence versus Classical Depolarization in Square and Hexagonal Nanohole Arrays. *Phys. Rev. A* 72, 013817, 1–5 (2005)
10. Altewischer, E., Ma, X., van Exter, M.P., Woerdman, J.P.: Fano-type Interference in the Point-Spread Function of Nanohole Arrays. *Opt. Lett.* 30, 2436–2438 (2005)
11. Altewischer, E., Ma, X., van Exter, M.P., Woerdman, J.P.: Resonant Bragg Scatter of Surface Plasmons on Nanohole Arrays. *New. J. Phys.* 8(57), 1–14 (2006)